NASA Technical Paper 1467

Miniature Flow-Direction and Airspeed Sensor for Airplanes and Radio-Controlled Models in Spin Studies

David D. Kershner

MAY 1979

NASA

NASA Technical Paper 1467

Miniature Flow-Direction and Airspeed Sensor for Airplanes and Radio-Controlled Models in Spin Studies

David D. Kershner
Langley Research Center
Hampton, Virginia

National Aeronautics
and Space Administration

**Scientific and Technical
Information Office**

1979

SUMMARY

A miniature flow-direction and airspeed sensor was developed for use on 1/10- to 1/15-scale models and on full-scale airplanes engaged in spin research. The range of flow angles encountered in spinning flight (±120° in angle of attack and ±55° in sideslip) is larger than that of normal flight. These angles along with an effective airspeed range of 9 to 90 m/sec, were measured with static accuracies of ±0.35° for angle of attack, ±0.25° for sideslip angle, and ±1 m/sec for airspeed. The dynamic accuracy is adequate to measure the rapidly changing flow angles and airspeed without significant distortion. The sensor is rugged enough to withstand both the airplane environment and that of the radio-controlled, unpowered models.

INTRODUCTION

A flow sensor to be used in spin testing of airplanes and radio-controlled models has been designed to be small in size and to have large angular ranges (±120° angle of attack and ±55° sideslip), a suitable airspeed range (9 to 90 m/sec), and suitable dynamic response (flat to 2 Hz). No commercially available sensor presently meets these requirements. The models, 1/15 to 1/10 of full size, are scaled in size, weight, and inertia so that the flight performance of the models is similar to that of the full-scale airplane. To this end, the additional moment added by the sensor about the pitch and yaw axes must be small. Standard components such as potentiometers and slip rings cannot be incorporated into a sensor without enlarging it to an unacceptable degree, so several critical components have been designed especially for the sensor. A low-inertia boom is long enough to place the sensor in relatively undisturbed air without introducing errors due to boom bending.

The configuration of the sensor is modeled after that of undocumented sensors designed for research on earlier models and on large parawing systems at the National Aeronautics and Space Administration (NASA). (See ref. 1.) A finned body containing a propeller anemometer is mounted on a fixed boom and rotates about two independent axes to self-align itself in the airstream (fig. 1). Potentiometers sense the flow angles, and the propeller anemometer in the body senses the airspeed. The swiveling design provides direct measurements of the large flow angles of spinning flight. The sensor is not designed for all-weather service. The requirements of range, accuracy, and dynamic response for the angular and airspeed measurements are given in table I. The design consideration and the performance of the sensor are discussed in this paper. A detailed description of the sensor construction is included in the appendix.

SYMBOLS

A	aspect ratio
a	slope of lift curve, rad^{-1}
f	frequency, Hz
g	acceleration of gravity, g units (1g = 9.8 m/sec^2)
I	mass moment of inertia, $kg\text{-}m^2$
i	propeller blade incidence, deg
$k_{1,2,3}$	constants of proportionality
l	distance from vane pivot to the vane aerodynamic center, mm
q	dynamic pressure, $\frac{1}{2}\rho U^2$, Pa
r	radius, mm
S	effective area of vane, mm^2
T	thickness of vane, mm
t	time, sec
U	approach airspeed, m/sec
V	velocity of vane element, m/sec
α	angle of attack, deg
ζ	damping ratio
ρ	density, kg/m^3
τ	time constant, sec

Subscripts:

A	of air
c	calibrated
n	natural
v	of vane

DESIGN CONSIDERATIONS

Static Angular Response

Angle of attack is measured in the plane containing both the longitudinal and normal axes, between the boom axis and the projection of the resultant wind vector on the plane (ref. 1). Sideslip angle is measured between the resultant wind vector and its projection on the same plane. The swiveling, streamlined aerovane self-aligns with the relative wind, and the potentiometers measure the two angles directly. The sensor is accurately made of rugged construction to provide precise and repeatable measurements with the high-resolution potentiometers. An accurate calibration fixture is needed for laboratory and field use.

Dynamic Angular Response

The aerovane body with cruciform X tail responds to dynamic aerodynamic inputs as a single-degree-of-freedom, second-order system with viscous and Coulomb damping. Both the spring force and the viscous damping force are generated by aerodynamic lift on the tail. The response of flow vanes has been described by several investigators (refs. 2, 3, and 4) in terms of the vane parameters. The undamped natural frequency relates to the various parameters by the equation

$$f_n = \frac{U}{2\pi}\left[\frac{\rho_A S}{2I}\,\frac{a\ell}{(1 + 2/A)}\right]^{1/2} \cong \frac{1}{2\pi}\left[\frac{qa}{\rho_V T \ell\,(1 + 2/A)}\right]^{1/2} \qquad (1)$$

The natural frequency is seen to increase as the inertia of the aerovane is reduced, which would be expected. The approximation of equation (1) neglects all inertia except that of the vanes and equates their radius of gyration to the aerodynamic moment distance ℓ. This is done to show that responsiveness is inversely proportional to the square root of, and not the first power of, the distance ℓ. It is also seen in equation (1) that the natural frequency varies as the square root of the dynamic pressure (i.e., the faster the flight, the greater the responsiveness), and that responsiveness is improved by using aerodynamically efficient vanes. Vane planforms were investigated in wind-tunnel tests. The planform selected (tapered, with an aspect ratio of 4) was found to be a good compromise between structural and aerodynamic characteristics. It produced acceptable stiffness and did not flutter in the airspeed range of interest.

Aerodynamic lift, in addition to forcing the alignment of the aerovane to the airstream, also provides damping force. This damping force, which is proportional to the tranverse velocity of the aerovane tail, should be made as high as possible. The damping ratio, defined as damping force divided by the minimum force needed to prevent overshoots in response to inputs, is shown by references 2, 3, and 4 to be

$$\zeta = k\left(\frac{\rho_A S a l^3}{I}\right)^{1/2} \cong \left(\frac{\rho_A}{\rho_v}\frac{a l}{T}\right)^{1/2} \tag{2}$$

Note that the damping ratio is independent of airspeed but dependent upon air density; that is, damping does not change with airspeed, only with altitude. The approximate form of equation (2) is obtained with the same assumptions of the approximate form of equation (1), and it shows that damping is improved by using low-density materials and by increasing the distance l. The effect of the distance l on the overall frequency response, which includes both natural frequency and damping, is best resolved by designing for high-frequency response at the expense of damping; however, the upper limit of natural frequency is set by the value of the first resonant frequency of the boom that is used to mount the sensor to the models. The boom and the vane form a two-degree-of-freedom vibration system that becomes divergent for the boom as the vane frequency approaches the first natural mode of the boom. Dangerous resonance is avoided in the scale-model application by limiting the natural frequency of the aerovane at the maximum airspeed to a value below the boom frequency. In airplane applications, the relatively larger booms with lower first-mode resonances are not subject to this condition.

Propeller Response

Propeller operation is described by considering the motion of the freely turning blade and that of the flow passing through it. When the blades neither receive nor deliver significant power to the airstream, as in the anemometer case, air passes through the propeller disc essentially undeflected; this is the no-slip case. The flat, untwisted blades rotate at speeds proportional to true airspeed throughout the range of interest and become nonlinear only at the slowest speeds where the mechanical load is significant and the blades slip to provide additional aerodynamic torque.

The velocity of the propeller blade is related to the true airspeed by the equation

$$V = U \tan\left(i - \frac{\rho_c}{\rho}\alpha\right) \tag{3}$$

This equation is impossible to evaluate because of the unmeasurable angle of attack α at low airspeeds, but the approximation

$$V = k_1 U + k_2\sqrt{\frac{\rho_c}{\rho}} \tag{4}$$

from reference 5 satisfactorily describes a linear relationship between the two velocities and an offset near the origin. Variation of air density affects the offset and not the slope of the calibration. The offset is smallest in dense air and increases with the lowering air density of higher altitude flight.

Airspeed data normally change slowly in most flight tests, but it can show dynamic changes when gusty air is encountered or abrupt maneuvers are executed. The propeller responds to dynamic inputs as a typical first-order system described by the equation

$$U = k_3 V + \tau \frac{dV}{dt} \tag{5}$$

Dynamic data are evaluated by adding the second term, which is the time constant times rate of change of airspeed, to the first term, which is measured airspeed.

PERFORMANCE CHARACTERISTICS

Systematic errors in angular measurements arise from nonlinearity of the potentiometers and misalignments in the airstream due to maneuver-generated accelerations or aerodynamic forces. Random errors affecting the angular measurements include friction-caused hysteresis and noise. Most of the nonlinearity error is removed in the data-reduction process by using piecewise linear fits to the angular calibrations. Precise balancing of the aerovane by the method described in the appendix assures that the aerovane will remain aligned during flight accelerations. No misalignments arising from aerodynamic forces were measured in wind-tunnel tests. Plastic resistive elements used in the potentiometers produce a nearly imperceptible level of noise. Discontinuities in the electrical outputs are eliminated by correctly setting the wiper tension when the sensor is assembled. Excessive hysteresis results from too much friction at the wiper contacts of both the potentiometers and the slip rings. The total friction is set to produce, in the absence of vibration, less than $\pm 0.25^{\circ}$ hysteresis in angle of attack and $\pm 0.10^{\circ}$ in sideslip angle at an airspeed of 30 m/sec. At higher airspeeds and in the presence of vibration, hysteresis disappears. Total uncorrected errors amount to $\pm 0.35^{\circ}$ in angle of attack and $\pm 0.25^{\circ}$ in sideslip angle.

Static airspeed calibrations (fig. 2) show that above 9 m/sec, the response is linear to within ± 0.5 m/sec. A detailed study of the calibration near the starting speed (fig. 3) shows the points asymptotically approach the straight slope as friction is overcome and the blades turn in proportion to the velocity of the inflowing air. The effect of changes in air density is to change the zero offset of the calibration with no change in the slope (ref. 5). The effect is small enough to be inconsequential under the altitude range of spin testing (ref. 6); therefore, no corrections are made to flight data for air-density changes. An overall airspeed accuracy of ± 1 m/sec is realized.

The dynamic angular response of the sensor in terms of natural frequency and damping ratio was measured from time-history records as the sensor responded to plucks at airspeeds of interest (fig. 4). The response is high enough for flight testing (table I) and yet low enough not to excite the first-mode resonance of the boom, 39 Hz, at the maximum airspeed.

The dynamic response of the airspeed sensor in terms of time constant was measured in an open-jet wind tunnel at several airspeeds from time-history

records of the output as the propeller was released in a constant-velocity airstream. The time constant was measured from a point v_1 at which the output had reached a reasonable value to the point at which it had reached 63 percent of the difference between v_1 and the final value. The time increment is the time constant and, as expected, was found to be independent of the reference value chosen. The relation between the measured time constants and the corresponding airspeeds (fig. 5) shows that the minimum acceptable lag is achieved for airspeeds exceeding 13 m/sec.

The rotational speed of the propeller drops off when it is not aligned with the airstream. The output of the sensor varies approximately as the square of the cosine of the angle of misalignment over the first 6° (fig. 6). This condition is considered satisfactory since large aerovane misalignments are not anticipated because of low friction in the bearings.

Tests to measure static angular and airspeed accuracies and dynamic response of the angles were made in the closed test section of the 0.305- by 0.43-m instrumentation wind tunnel. Tunnel speeds were sensed with a pitot static tube located near the sensor. Pitot and static presures were measured with an accuracy of ±13.3 Pa (0.01-mm Hg) or less, and the tachometer-output frequencies were measured with a frequency counter to an accuracy of ±1 Hz.

Flight experience has proven the sensor to be reliable and rugged. In over 100 flights of radio-controlled, unpowered models, only one loss of data has occurred. Airplane service has proven more difficult because the vibration environment is more severe and the duty period is longer, but failures have only occurred as a result of lapses in the quality of preparation.

CONCLUDING REMARKS

A miniature flow-direction and airspeed sensor was developed for both scale models and full-scale airplanes engaged in spin research. The large flow angles encountered in spinning flight (±120° in angle of attack and ±55° in sideslip angle) are measured to an accuracy of ±0.35° and ±0.25°, respectively. True airspeed is measured over a range of from 9 to 90 m/sec to an accuracy of ±1 m/sec. The dynamic response of the sensor is adequate to measure the rapidly changing flow angles without significant distortion. The sensor has proved rugged enough to withstand both the airplane environment and that of the radio-controlled, unpowered free-flight models.

Langley Research Center
National Aeronautics and Space Administration
Hampton, VA 23665
April 24, 1979

APPPENDIX

DESCRIPTION OF SENSOR

General Description

The sensor is shown disassembled in figure A1. The sensor is mounted on a support boom that fits to the nose of the model or airplane. The major parts of the sensor are the supporting stationary housing (pod), the rotating cross-shaft, and the swiveling aerovane. These three parts, plus the other parts and components of the sensor, are shown in approximately correct position in figure A1. The aluminum, two-piece housing on the left contains the bearings that support the cross-shaft, the annular-shaped potentiometer with the single-element wiper, and the seven-element slip-ring assembly. The potentiometer is fastened to the shaft, rotates with it, and senses angle of attack. The slip-ring assembly likewise is fastened to and rotates with the shaft. The cross-shaft is made of stainless steel and is bored to contain the electrical wires. Each wire enters the shaft through one of five radial holes; all five emerge together on the outer end. A yoke which supports the aerovane is attached to the outer end. The shaft running through the yoke is long enough to support bearing assemblies which fit into the halves of the aerovane when it is assembled. The sideslip potentiometer and the three-element slip ring are mounted on the shaft between the ends of the yoke. The shaft, potentiometer, and slip rings are stationary relative to the cross-shaft and yoke, but the aerovane rotates in the bearings. The wipers for both the sideslip potentiometer and the small slip rings are mounted in the aerovane and turn with it around the shaft. The complex shape of the aerovane interior results from the need to miniaturize. The nose of the aerovane contains a propeller-tachometer assembly which rotates to produce a sinusoidal electrical output with a frequency proportional to true airspeed. The lightweight tail is made of thin magnesium sheets fitted into slots in a shaft which is inserted into the aerovane body to a depth that provides static balance. The lengths of the tail and cross-shaft and the size of the cutout in the side of the aerovane allow rotation through a sideslip range of $\pm 55^{\circ}$. There are no stops to limit the rotation of the cross-shaft in the angle-of-attack axis. Electrical connections are made to the various components through the slip rings. Two wires from the tachometer and the wiper wire from the potentiometer attach to the wipers of the slip-ring assembly in the aerovane. These three, plus the two wires from the ends of the sideslip potentiometer, pass through the cross-shaft to the slip-ring assembly in the housing where the two wires from the ends of the angle-of-attack potentiometer are also attached. These seven wires, plus the one wire from the wiper of the angle-of-attack potentiometer, are passed through the housing and the hollow mounting boom to the recording instrumentation inside the model or airplane. Some of the parts and components are described in greater detail in the following sections.

Propeller-Tachometer Assembly

The propeller shown in figure A2 is molded of aluminum alloy by an investment-casting technique. The streamlined hub, which is a continuation of

the body shape, is hollow except for the material provided for the mounting shaft and the web strengtheners. The flat blades are 31.75 mm in diameter, 7.6 mm in chord, and 0.51 mm thick. They are set at an incidence angle of 13° to give the desired maximum rotational speed (18 000 rpm) at the maximum airspeed of 90 m/sec.

The tachometer subsystem (fig. A2) is composed of a magnetic pickup and a rotating, six-toothed mild-steel pole piece. The pole piece and propeller rotate together on the common shaft that is supported by low-friction, shielded ballbearing assemblies. The spacing between the magnetic pickup and the pole piece is adjusted to approximately 0.38 mm. The rotation produces a sine-wave output at the desired voltage level without undue magnetic drag at the minimum airspeed. The magnetic pickup is a commercially produced item which has an inductance of 14 mH, a dc resistance of 140 Ω, and an output of approximately 0.30 V root mean square at 300 rps, which is the maximum speed. The mechanical load presented to the propeller by the tachometer consists of the friction torque in the bearings and the magnetic torque of coupling between the pickup and the rotating pole pieces. The loads cause a threshold of rotation and nonlinearity in the relation between airspeed and rotational speeds at airspeeds below the range of interest. The assembly is identical to the one described in reference 6.

Cross-Shaft

The cross-shaft mechanically and electrically connects the aerovane with the stationary housing. The shaft is shown in figure A3, along with some of the associated components. It is drilled axially from the yoke end to the depth where the wires are brought through five radially drilled holes to the slip-ring assembly. The diameter of the shaft is large enough to limit bending to less than 1/4° under 6g acceleration, the maximum expected during flight. Additionally, the shaft is capable of supporting the aerovane without bending past its elastic limit during model landing impact, which is approximately 50g. The shaft material, precipitation-hardened stainless steel, has a tensile yield strength of over 10.0×10^6 N/m^2 and many desirable qualities such as corrosion resistance, weldability, stability during heat processing, machinability, and lack of brittleness.

Slip Rings and Potentiometers

The slip rings are custom-made by a commerical supplier to fit the sensor. The rings are rhodium-plated silver and the wiper metal is a palladium alloy, both of which are materials customarily used for slip-ring applications. The contact pressure between each wiper and ring is adjusted at the time of sensor assembly by bending the wipers. As excessive friction causes wear and impairs free rotation of the aerovane, care must be taken to provide uniform pressures in the amount needed to assure electrical contact. The potentiometers (fig. A4) are custom-made by a commercial supplier according to detailed drawings and are made of polyimide plastic. The resistive element is attached in the desired areas and is reduced in width as needed to provide the required resistance and

linearity. Resistive elements are applied to the rims of the angle-of-attack bodies over the range of ±120° and to the faces of the sideslip bodies over a ±55° range. The resistance of both potentiometers is 5000 Ω, ±5 percent, and is linear over the range to within ±1.5 percent of range. Resolution of the potentiometers is infinite except for noise. Noise, which is due to surface irregularities, amounts to ±0.1 percent of full-scale range or less. With 6-V excitation, the potentiometers dissipate less than 10 mW of electrical power. The wipers are of precious metal alloy mounted in separate molded polyimide blocks. Electrical continuity is made between the solder terminals and the resistive elements with conductive epoxy cement and lengths of small-diameter copper wire. The potentiometers are assembled in the sensor on their respective axes, the wiper blocks installed in their respective locations, and the amount of contact pressure adjusted as with the slip rings. Optimum friction gives good potentiometer life and performance.

Tail

Dynamic performance of the sensor depends to a great extent on the design of the tail; low inertia gives high natural frequency and damping. The vanes are made of 0.5-mm-thick magnesium alloy, interlocked, and set in slots cut in the 3.2-mm-diameter magnesium rod. The vanes are set normal to each other in an X-orientation. This orientation minimizes the effects of the wake from the cross-shaft on the aerovane and allows the tail greater clearance in the extreme position of sideslip as it approaches the cross-shaft and support boom.

Support Boom

The support boom (fig. A5(a)) was designed to support the sensor at the required distance ahead of the scale models while adding a minimum amount of inertia to them, to bend no more than 1/4° when subjected to the maximum acceleration load, 6g, expected during the data period, and to survive ground impacts of up to 50g. The boom is drilled to receive the wires from the sensor so that they can be routed to the recording instrumentation in the interior of the model. A key in the mounting hole mates with the keyway in the boom to orient both it and the sensor in alignment with the reference axes of the model to within ±0.2° in all axes. Full-scale airplanes require longer booms, but since each installation is unique, a standard boom was not developed. A typical wing installation is shown in figure A5(b).

Calibration Fixture

A fixture for calibrating the angles was designed for laboratory and field use (fig. A6). It can be attached with two thumb screws to the thin cylindrical section of the mounting boom around the roll axis and subsequently aligned with the angle-of-attack and slideslip axes. It can be seen in figure A6 that the fixture is configured to calibrate one axis at a time, with scales engraved in 1° increments. The fixture is lightweight and provides calibrated inputs that are accurate to within ±0.2° of the intended values.

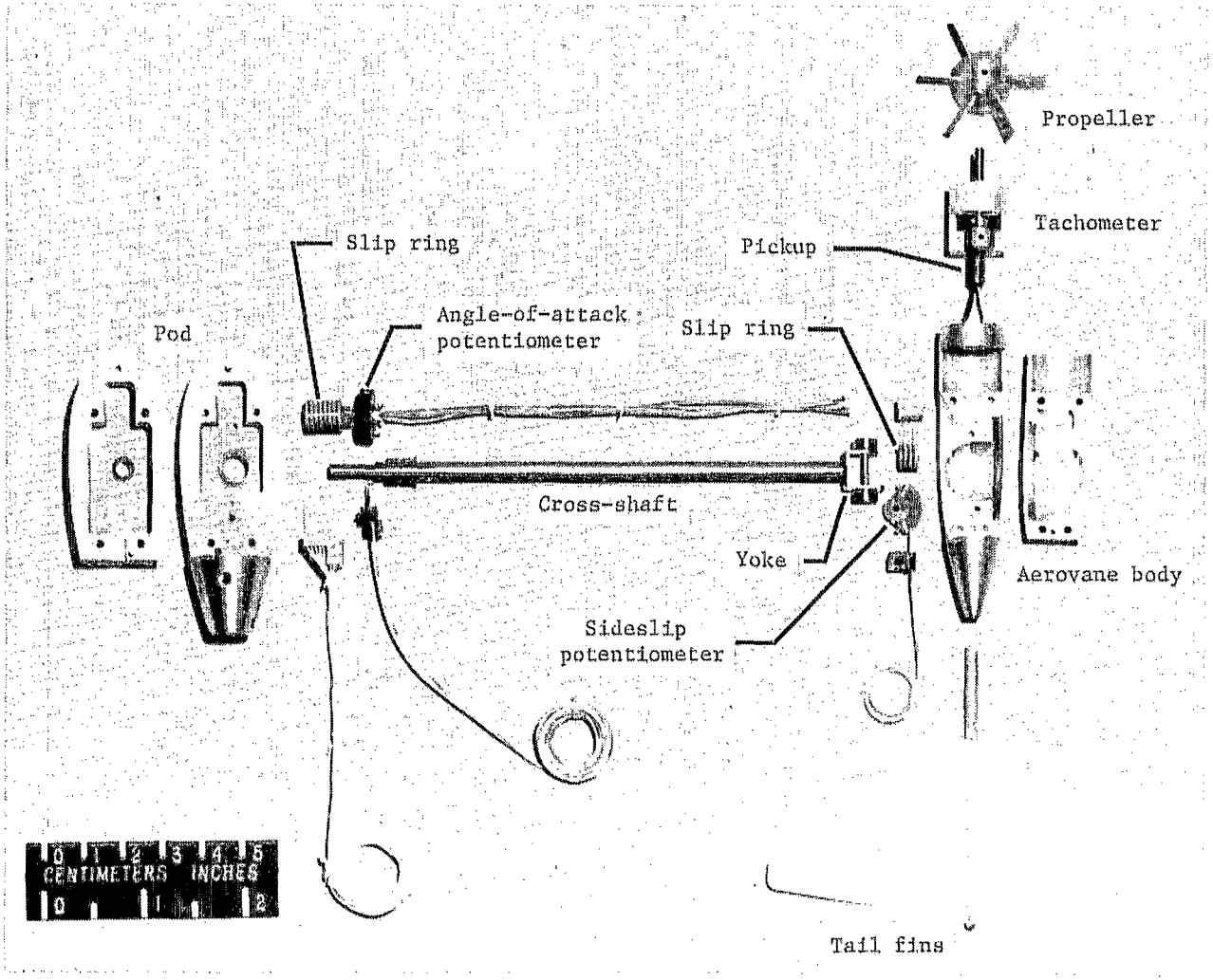

Figure A1.- Layout of components.

L-74.8557.1

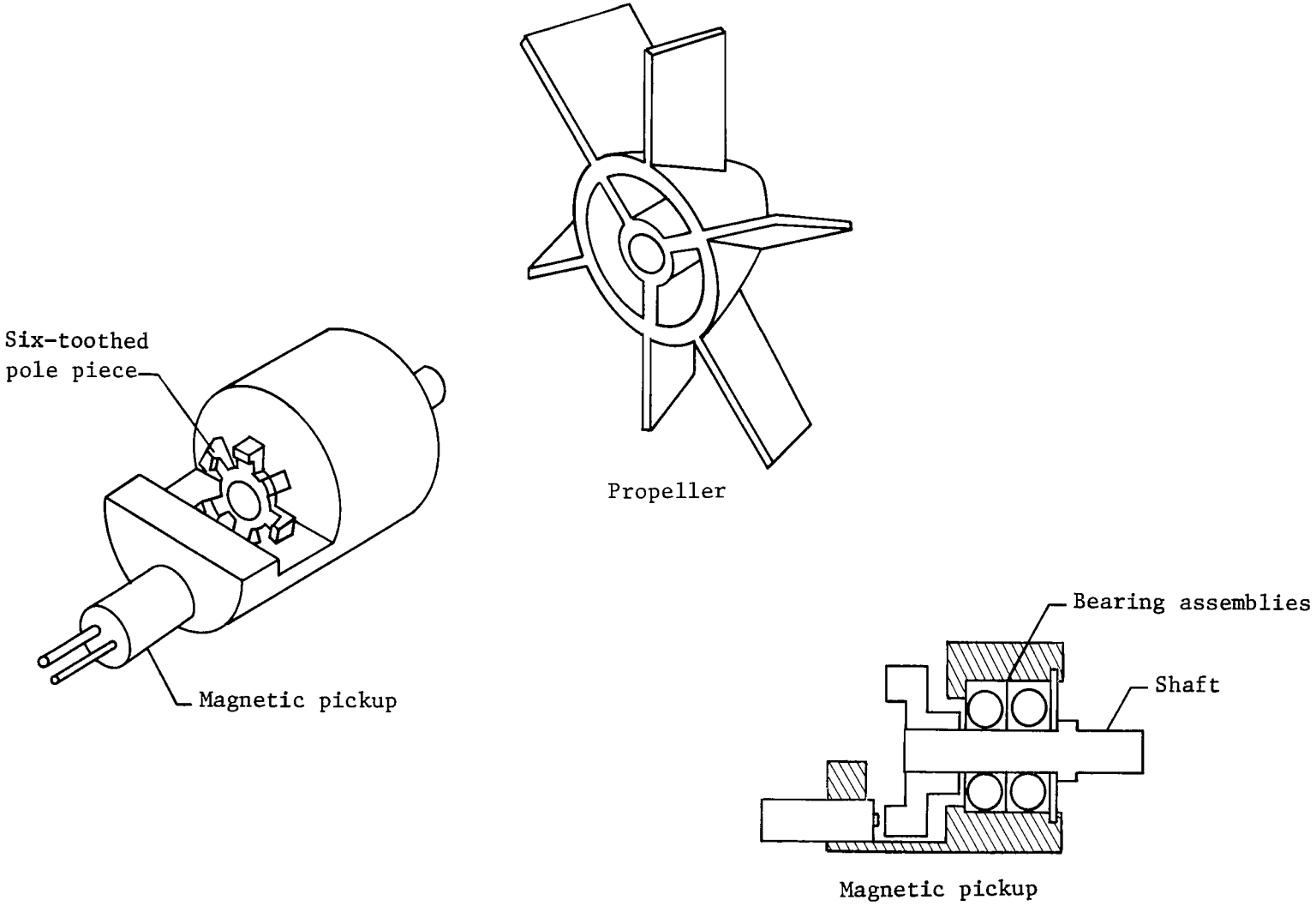

Figure A2.- Propeller-tachometer details.

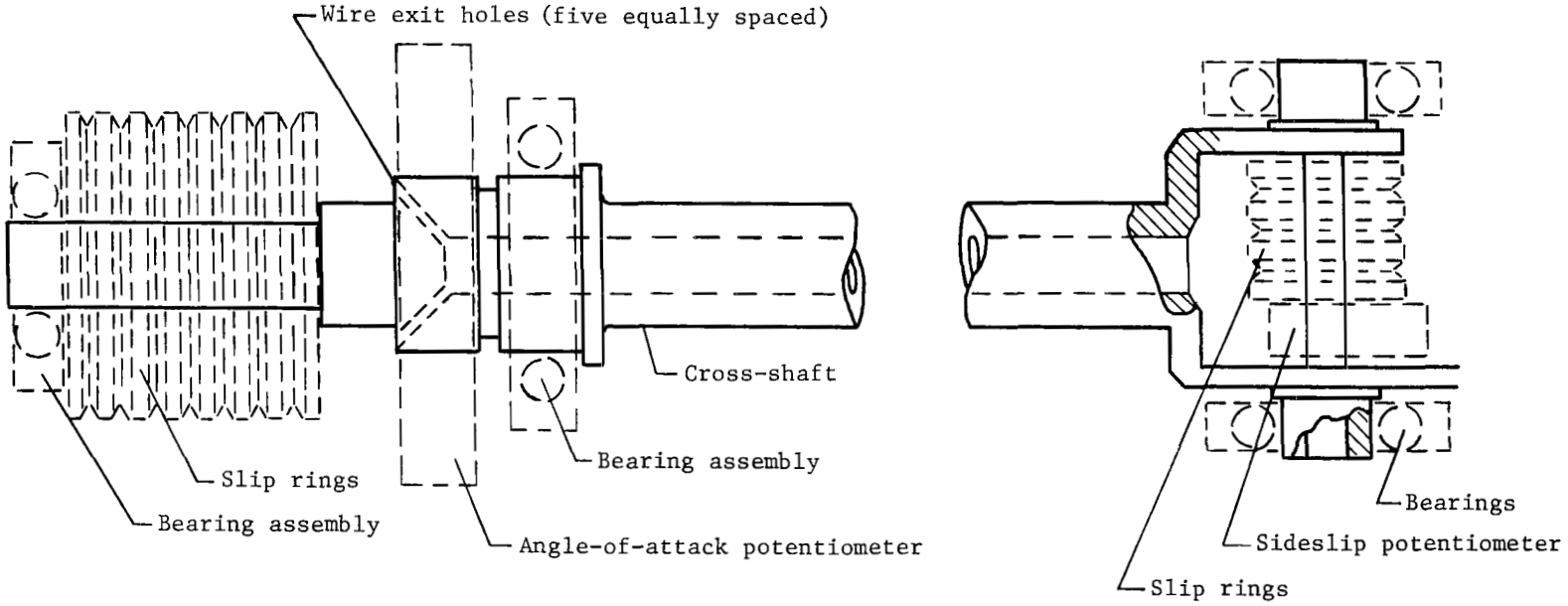

Figure A3.- Cross-shaft details.

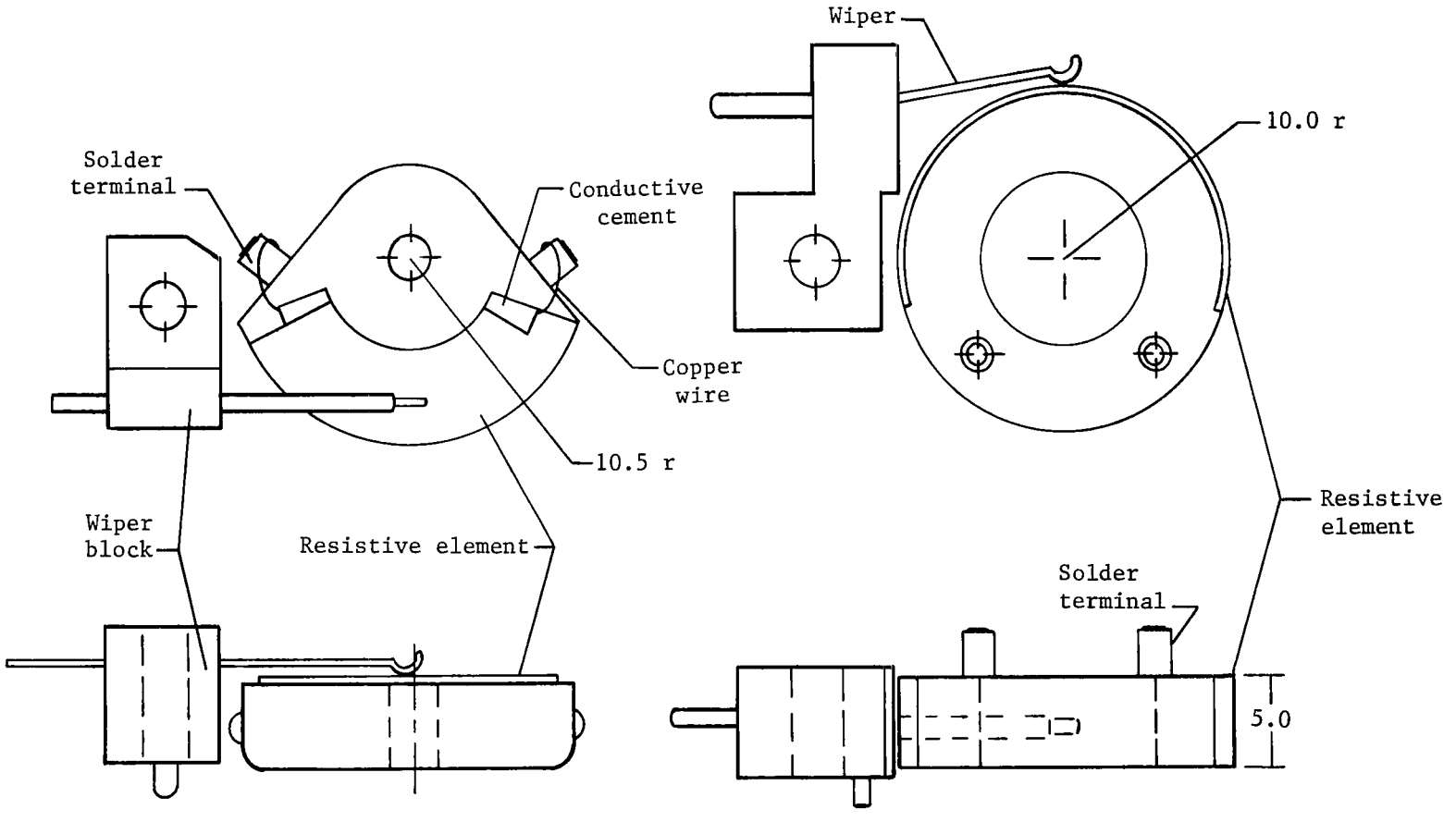

Figure A4.- Potentiometers. All dimensions given in millimeters.

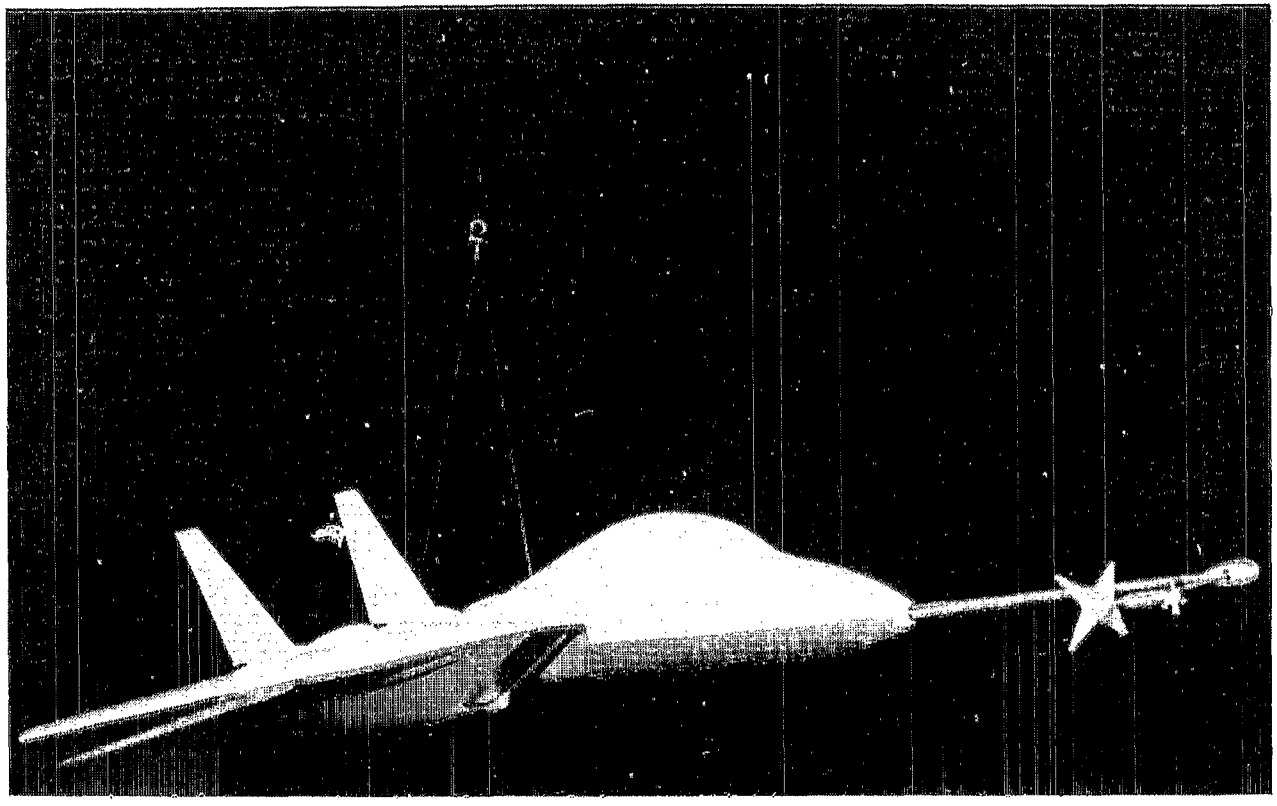

L-71-7567

(a) Drop model (F-14 model).

Figure A5.- Boom installation.

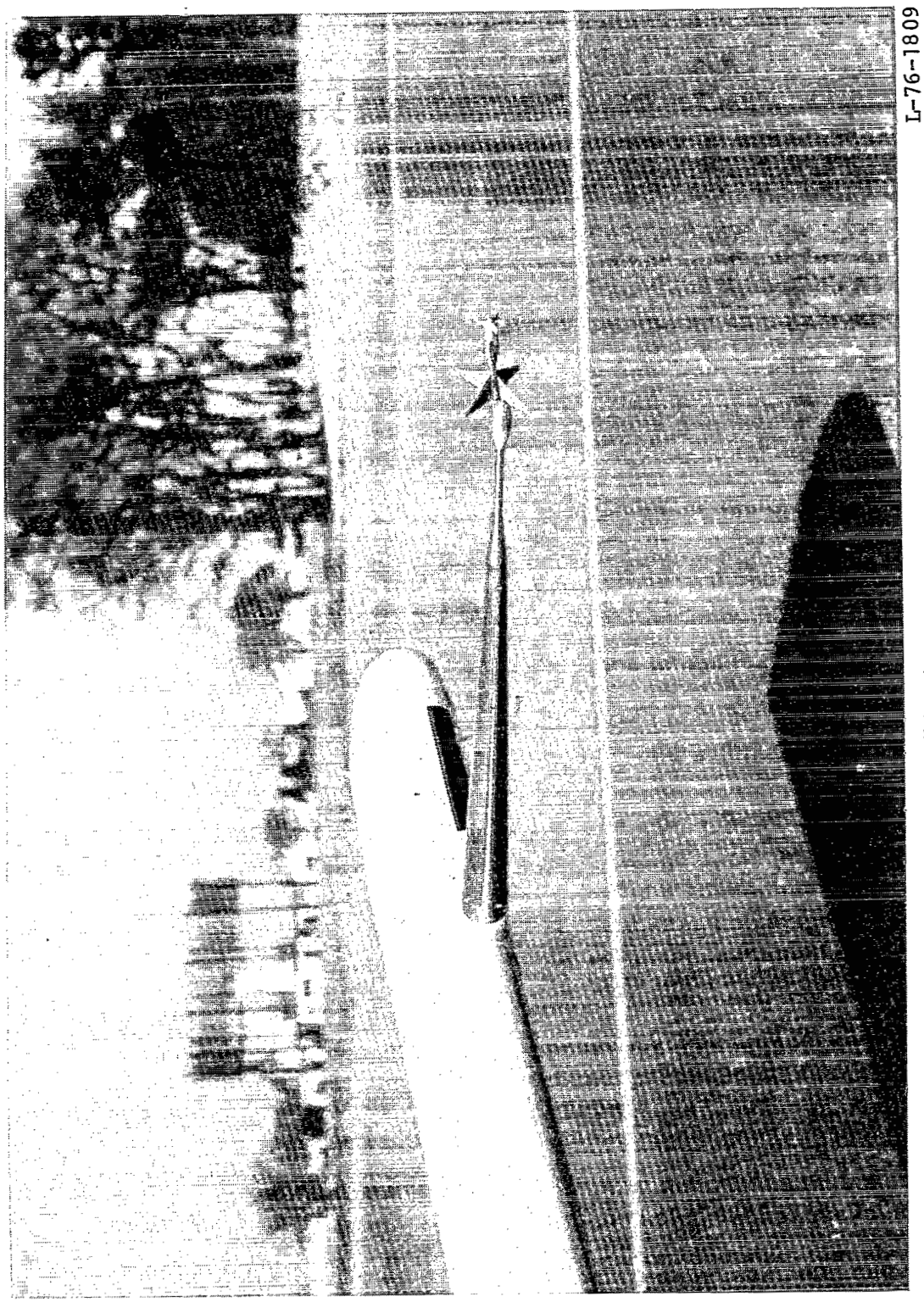

L-76-1809

(b) Aircraft.

Figure A5.- Concluded.

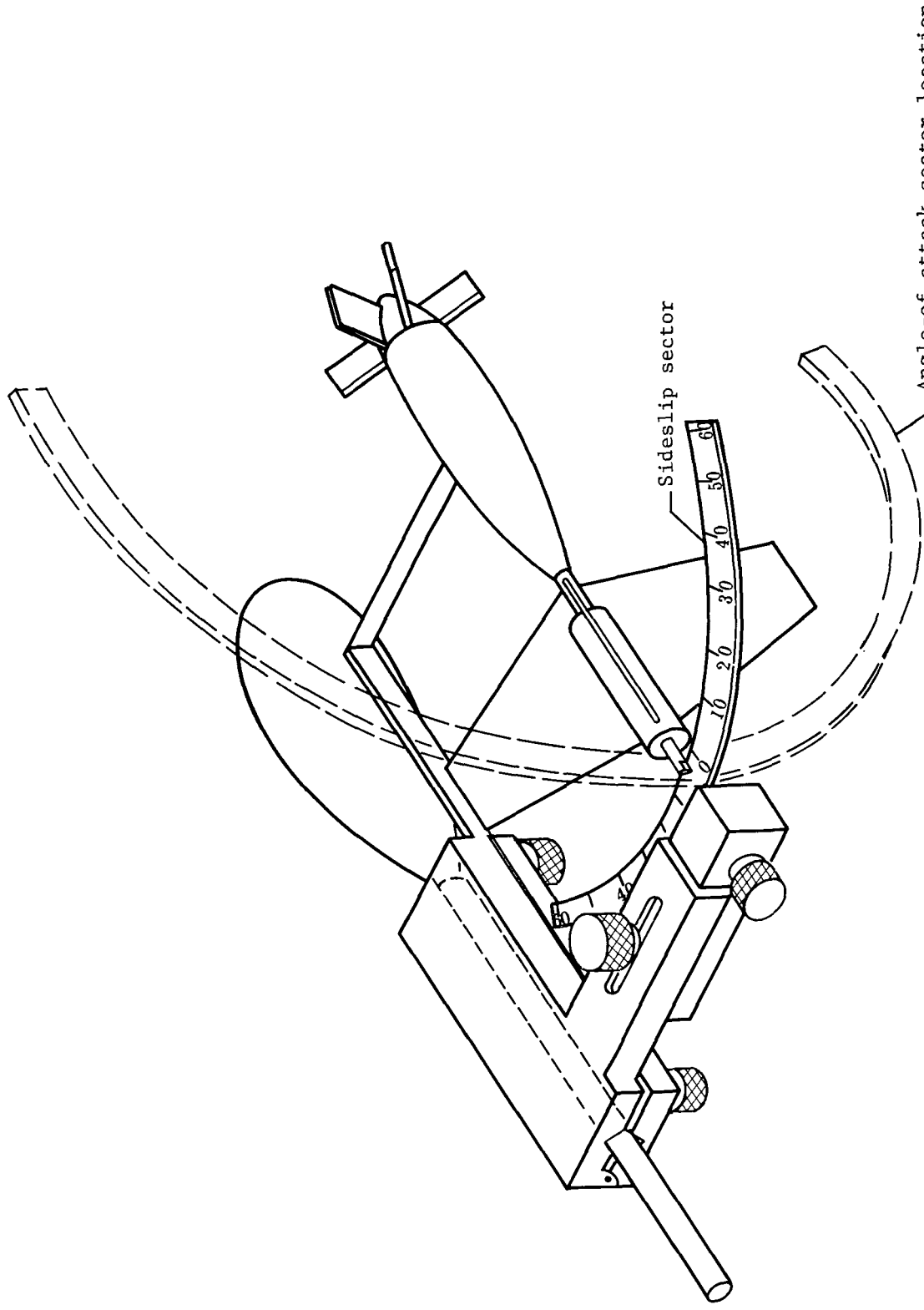

Figure A6.- Calibration fixture in place.

REFERENCES

1. Neihouse, Anshal I.; Klinar, Walter J.; and Scher, Stanley H.: Status of Spin Research for Recent Airplane Designs. NACA TR R-57, 1960. (Supersedes NACA RM L57F12.)

2. Barna, P. S.; and Crossman, Gary R.: Experimental Studies of the Aerodynamic Performance and Dynamic Response of Flow Direction Sensing Vanes. NASA CR-2683, 1976.

3. Wieringa, J.: Evaluation and Design of Wind Vanes. Appl. Meteorol., vol. 6, no. 6, Dec. 1967, pp. 1114-1122.

4. MacCready, Paul B., Jr.; and Jex, Henry R.: Response Characteristics and Meteorological Utilization of Propeller and Vane Wind Sensors. J. Appl. Meteorol., vol. 3, no. 2, Apr. 1964, pp. 182-193.

5. Ower, E.: The Measurement of Air Flow. Third ed., Chapman & Hall, Ltd. (London), 1949.

6. Kershner, David D.: A Suspended Anemometer System for Measuring True Airspeed on Low-Speed Airplanes. NASA TN D-8523, 1977.

TABLE I.- MEASUREMENT REQUIREMENTS

Parameter	Range	Accuracy	Frequency response
Angle of attack	±120°	[a]±0.35°	Flat to 2 Hz
Sideslip angle	±55°	[a]±0.25°	Flat to 2 Hz
Airspeed	9 to 90 m/sec	±1 m/sec	lag ≦ 0.1 sec

[a]This value includes random errors such as resolution, hysteresis, and repeatability, but does not include systematic errors such as nonlinearity or errors introduced by the recording system.

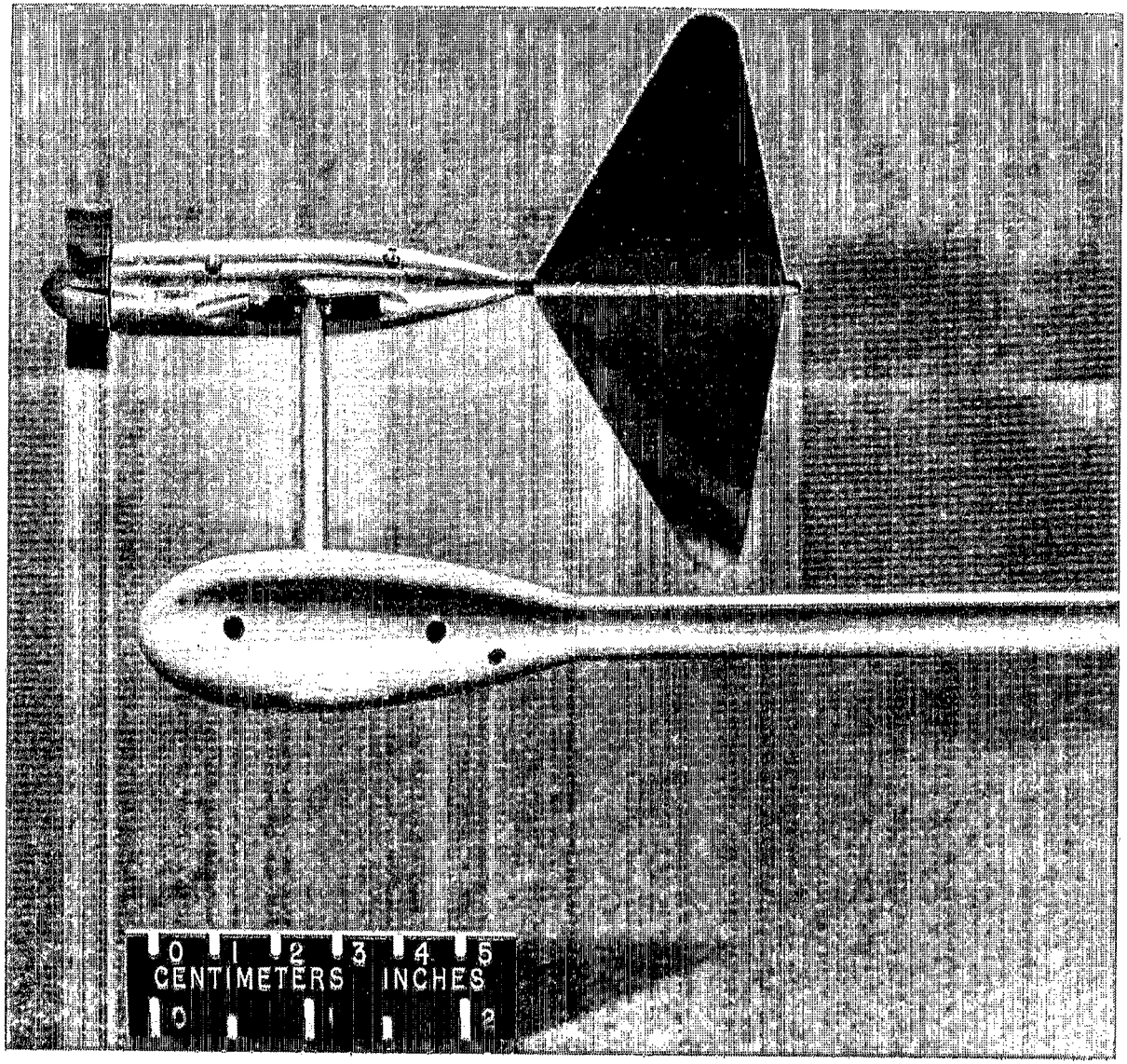

L-74-8558

(a) Side view.

Figure 1.- Flow-direction and velocity sensor.

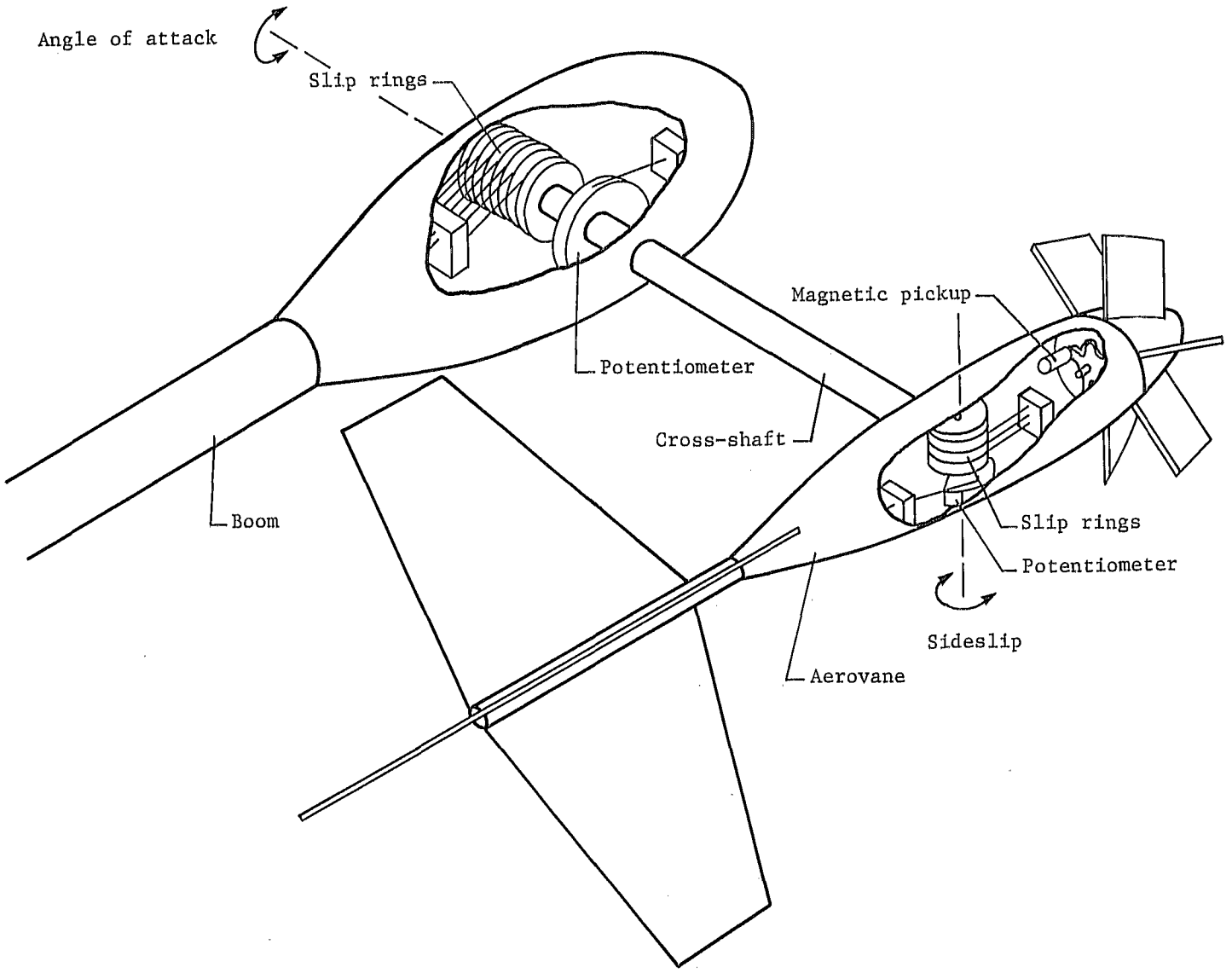

(b) Schematic.

Figure 1.- Concluded.

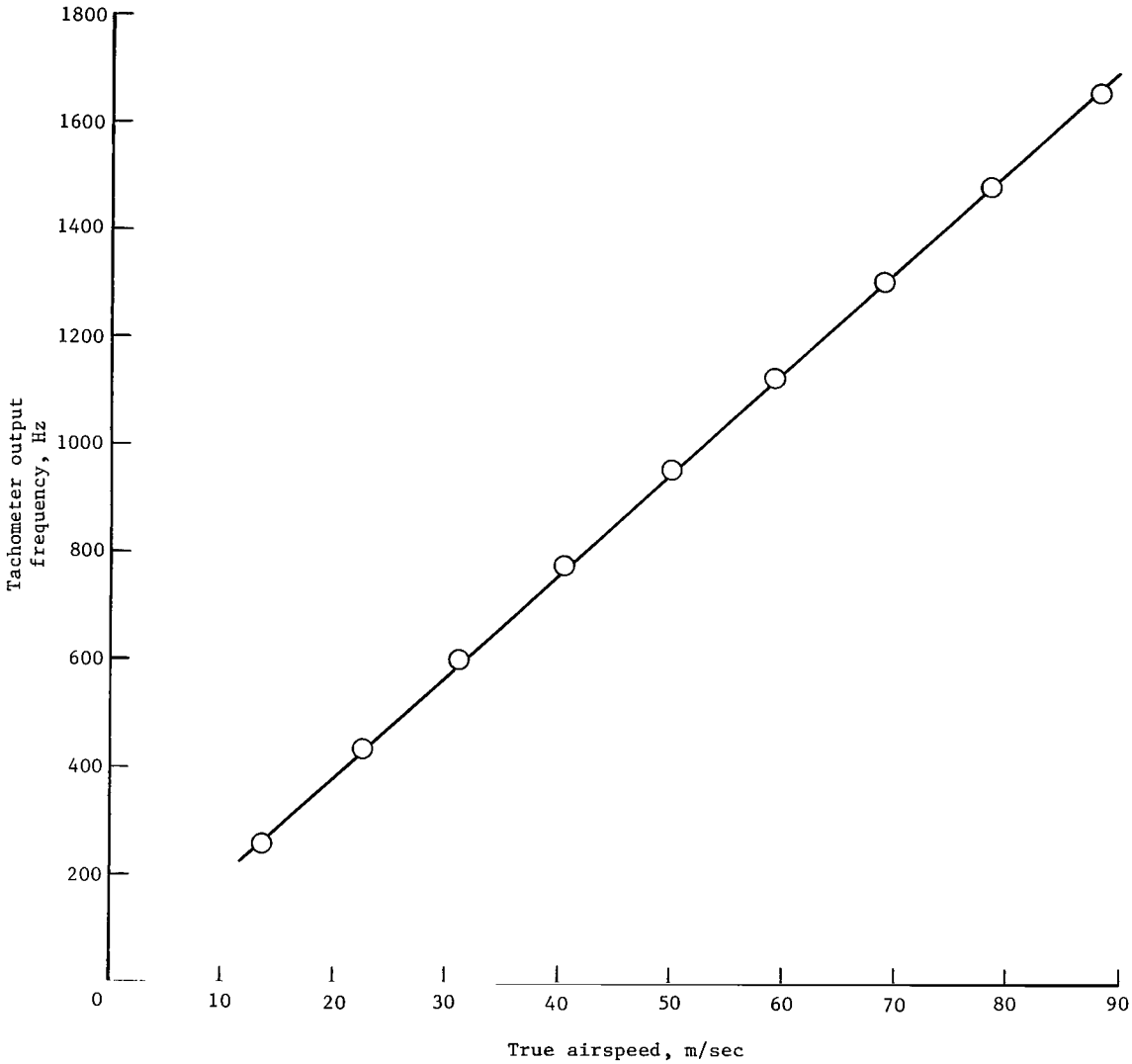

Figure 2.- Typical airspeed calibration.

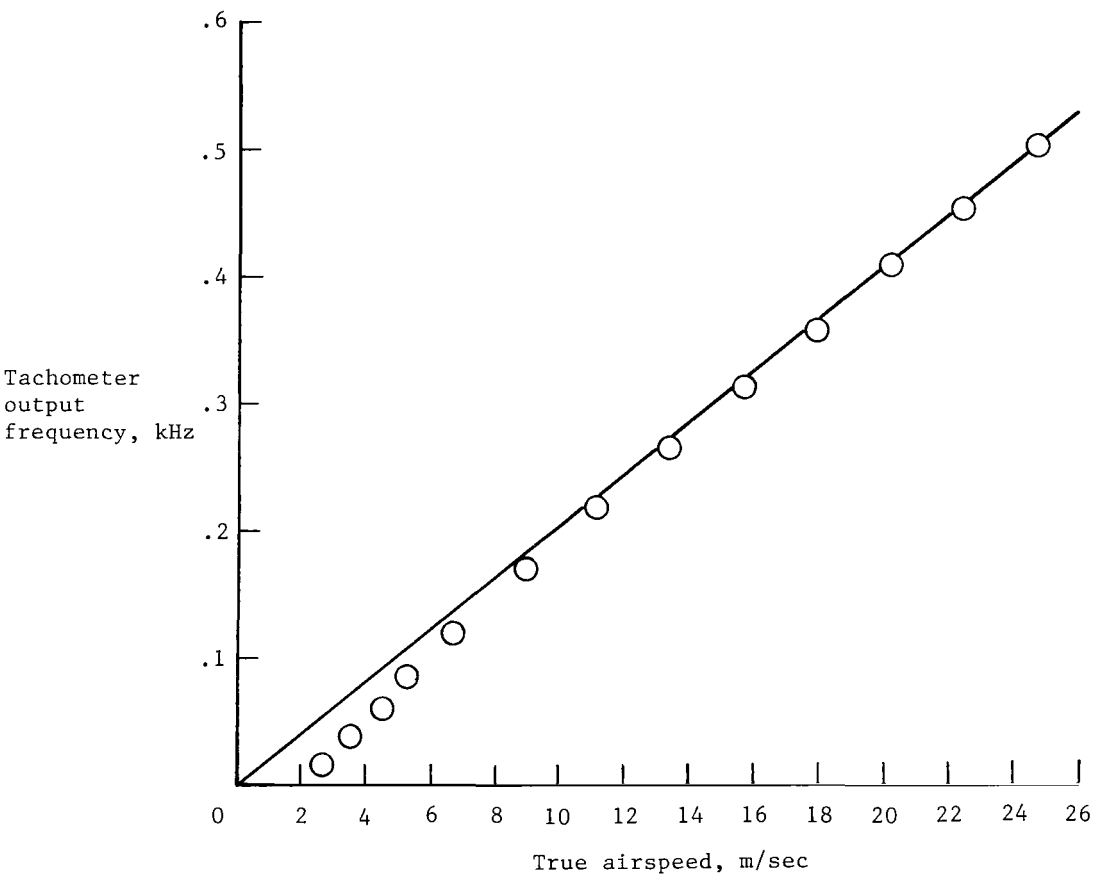

Figure 3.- Detailed calibration showing starting characteristics at sea-level conditions.

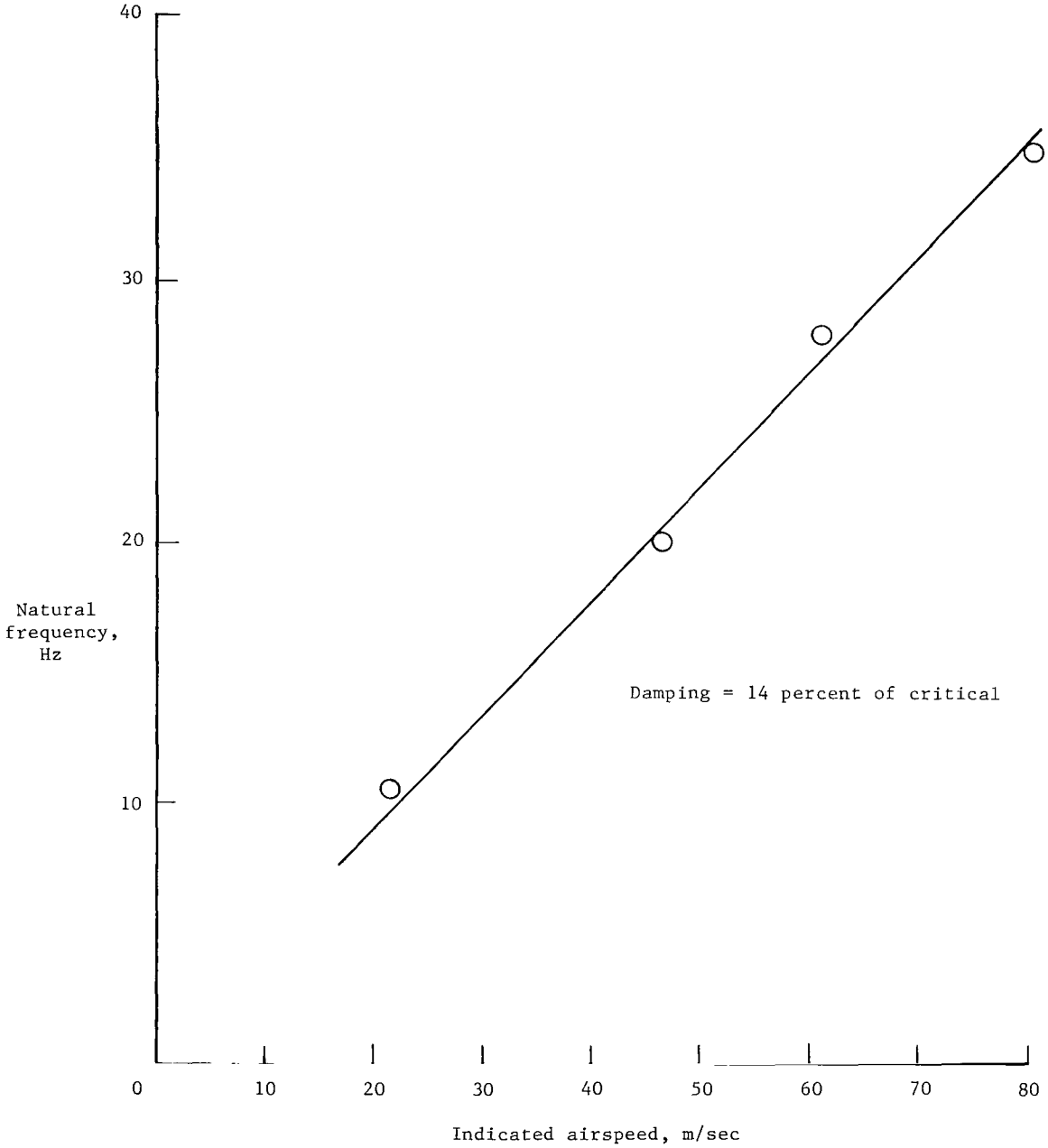

Figure 4.- Frequency response of angular measurements at sea-level conditions.

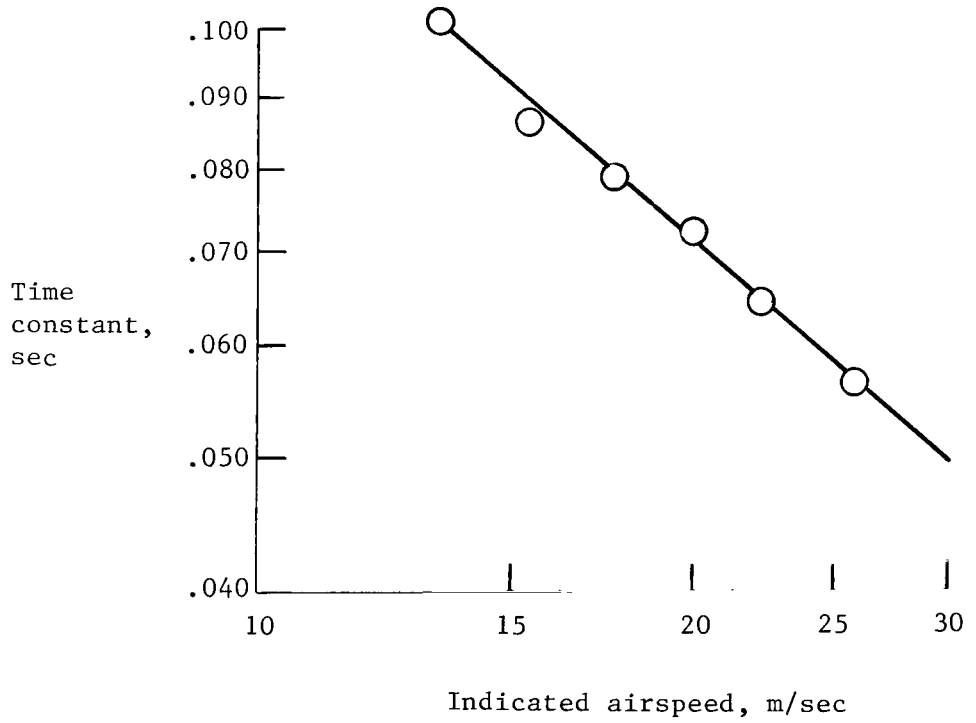

Figure 5.- Variation of anemometer time constant with indicated airspeed at sea-level conditions.

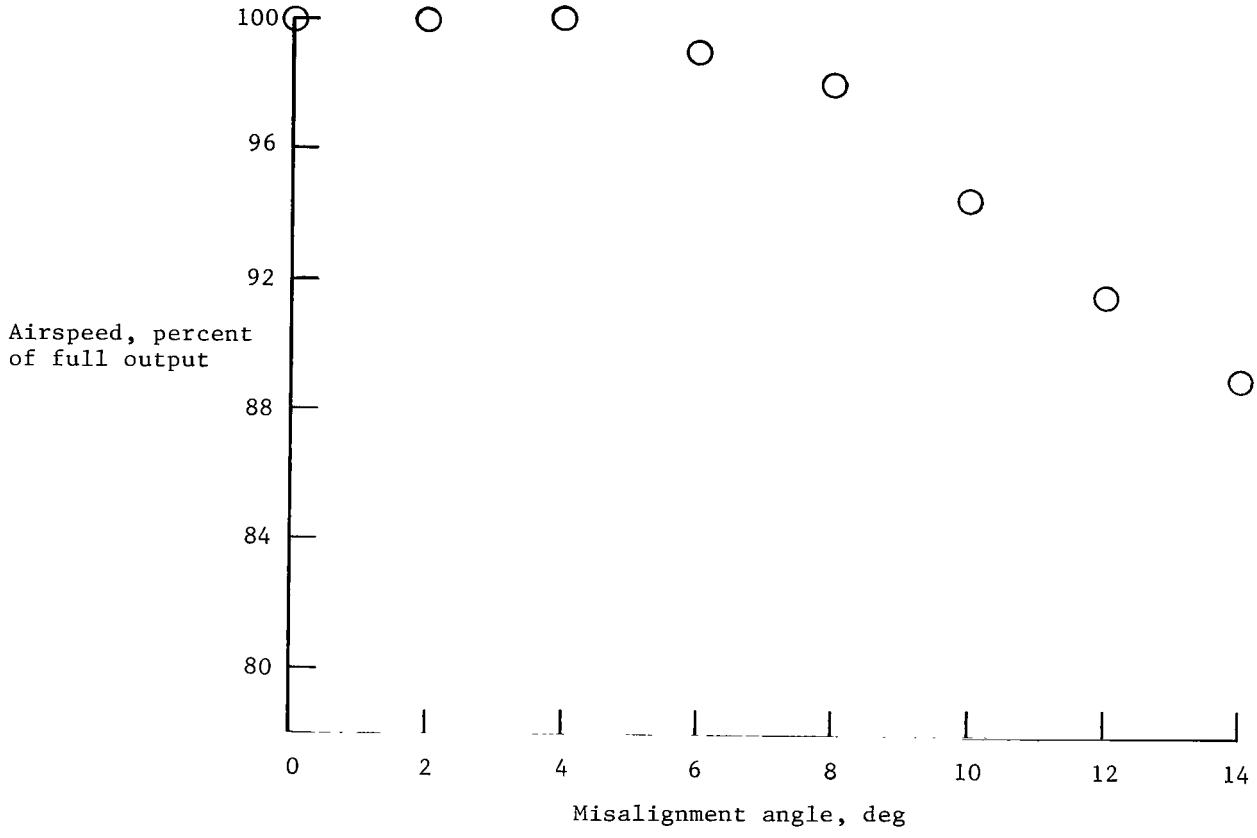

Figure 6.- Airspeed measurement variation due to misalignment. Data taken at airspeed of 17.4 m/sec at sea-level conditions.

1. Report No.	2. Government Accession No.	3. Recipient's Catalog No.
NASA TP-1467		

4. Title and Subtitle	5. Report Date
MINIATURE FLOW-DIRECTION AND AIRSPEED SENSOR FOR AIRPLANES AND RADIO-CONTROLLED MODELS IN SPIN STUDIES	May 1979
	6. Performing Organization Code

7. Author(s)	8. Performing Organization Report No.
David D. Kershner	L-12812

9. Performing Organization Name and Address	10. Work Unit No.
NASA Langley Research Center Hampton, VA 23665	505-10-13-04
	11. Contract or Grant No.

12. Sponsoring Agency Name and Address	13. Type of Report and Period Covered
National Aeronautics and Space Administration Washington, DC 20546	Technical Paper
	14. Sponsoring Agency Code

15. Supplementary Notes

16. Abstract

A miniature flow direction and airspeed sensor was developed for use on 1/10- to 1/15-scale models and on full-scale airplanes engaged in spin research. The range of flow angles encountered in spinning flight ($\pm 120^{\circ}$ in angle of attack and $\pm 55^{\circ}$ in sideslip) is larger than that of normal flight. These angles, along with an effective airspeed range of 9 to 90 m/sec, were measured with static accuracies of $\pm 0.35^{\circ}$ for angle of attack, $\pm 0.25^{\circ}$ for sideslip angle, and ± 1 m/sec for airspeed. The dynamic accuracy is adequate to measure the rapidly changing flow angles and airspeed without significant distortion. The sensor is rugged enough to withstand both the airplane environment and that of the radio-controlled, unpowered models.

17. Key Words (Suggested by Author(s))	18. Distribution Statement
Angle of attack Sideslip angle Airspeed Instrumentation Flow measurement	Unclassified - Unlimited Subject Category 06

19. Security Classif. (of this report)	20. Security Classif. (of this page)	21. No. of Pages	22. Price*
Unclassified	Unclassified	25	$4.00

* For sale by the National Technical Information Service, Springfield, Virginia 22161

NASA-Langley, 1979

5 1 1U,A, 051179 S00903DS
DEPT OF THE AIR FORCE
AF WEAPONS LABORATORY
ATTN: TECHNICAL LIBRARY (SUL)
KIRTLAND AFB NM 87117